communications biology

Article

https://doi.org/10.1038/s42003-024-06837-8

Delta wing design in earliest nektonic vertebrates

Check for updates

Héctor Botella [1], Richard A. Fariña[2] & Francisco Huera-Huarte [3]

The colonization of the pelagic realm by the vertebrates represents one of the major transitions in the evolutionary success of the group and in the establishment of modern complex marine ecosystem. It has been traditionally related with the Devonian rise of jawed vertebrates, but new evidences indicate that first active swimmers, invading the water column, occurred within earlier armoured jawless fishes ("ostracoderms"). These "primitive" fishes lacked conventional fish control surfaces and the precise mechanism used to generate lift and stabilizing forces still remains unclear. We show that, because of their shape, the rigid cephalic shield of Pteraspidiformes, a group of Silurian-Devonian "ostracoderms", generate significant forces for hydrodynamic lift. Particle Image Velocimetry and force measurements in a water channel shows that the flow over real-sized Pteraspidiformes models is similar to that over delta wings, dominated by the formation of leading-edge vortices resulting in enhanced vortex lift forces and delayed stall angles of attack. Additionally, experiments simulating ground effect show that Pteraspidiformes present better hydrodynamic performance under fully pelagic conditions than in a benthic scenario. This suggests that, lacking movable appendages other than the caudal fin, leading-edge vortices were exploited by earliest vertebrates to colonize the water column more than 400 Mya.

Delta wings are swept-back wings with a triangular planform used in a variety of aircraft, such as several aerospace vehicles and most modern fighters. They are extensively studied in the field of aerospace engineering due to their ability to provide considerable lift forces even at high angles of attack, which leads to a better aircraft stability and control characteristics compared to high-aspect-ratio wings, commonly found in commercial aircraft. The flow over a delta wing is characterized by a pair of counter-rotating leading-edge vortices (LEVs). LEVs in delta wings are a source of lift, as they induce a region of low pressure that yields a strong suction force on the wing's upper surface. This results in an additional lift, termed vortex lift, which can contribute as much as 40% of the total lift[1]. Nevertheless, at a critical angle of attack, LEVs experience a sudden disorganization with a dramatic expansion of vortex cores, known as vortex breakdown, which results in a rapid loss of lift and ultimately in stall[1–3].

Although, as far as we know, delta wings typical of aircraft are not biologically inspired, it is currently well-known that exploiting forces generated by LEVs is widespread among living beings. Thus, lift generated by LEVs is used by insects[4–7], bats[8,9], and birds[10,11] during flight, as well as by autorotating plant seeds during descent[12]. In addition, aquatic animals such as boxfishes[13,14] and some foot propelled swimming birds[15], employ the forces generated by the LEVs for trim control, promote maneuverability and/or propulsion. Nevertheless, in most of these cases LEVs are generated by moving appendages and not by stationary configurations as delta wings. In fact, flyers and swimmers that glide using fixed delta wing geometries are not common in nature, even though some examples resembling delta wing configurations have been reported in avian tails[16] and extinct gliding reptiles[17]. Interestingly, during Silurian to early Devonian times (more than 400 million years ago) delta-shaped headshields convergently evolved in several "ostracoderms" lineages including heterostracans, galeaspids, osteostracans, and pituriaspids[18,19]. "Ostracoderms" are a paraphyletic group of primitive jawless fishes that inhabited during Lower and Middle Paleozoic[18–20] representing the earliest vertebrate lineages. They lacked paired and median fins, except for the caudal one, and, in most of them, the anterior part of their bodies was enclosed in a large, rigid external bone shield. This rather primitive anatomy has posed doubts about their locomotion capabilities. Thus, traditionally, "ostracoderms" had been interpreted as bottom-living forms with restricted swimming capabilities[21–25], and the nektonic forms first evolved within jawed vertebrates linked with the emergence of other anatomical innovations, such as paired appendages[22,23,26–28]. In this sense, inspiring initial studies based on evidences

[1]Unidad de Paleobiología y Biología Teórica. Instituto Cavanilles de Biodiversidad y Biología Evolutiva, Universitat de Valencia, Valencia, Spain. [2]Departmento de Paleontología, Facultad de Ciencias, Universidad de la República, Montevideo, Uruguay. [3]Department of Mechanical Engineering, Universitat Rovira i Virgili, Tarragona, Spain. e-mail: francisco.huera@urv.cat

from fossil-diversity analysis suggest that jawed vertebrate nektonic forms, became highly diverse towards the end of the Devonian during the so-called "*Devonian Nekton Revolution*" (a major macroevolutionary event representing the sudden occupation of the water column[27], but latter re-analysis evidence that nekton and eunekton were well established prior to Devonian times[29]. In fact, evidence from different approaches indicate that, even though the shallow benthos was the ancestral habitat of vertebrates, earliest agnathan lineages reached a great ecological diversification during the Silurian, including the first pelagic vertebrate forms, well adapted to live in the water column[19,30–34]. Nevertheless, lacking conventional fish control surfaces, i.e. paired or unpaired median fins[35], or other conventional buoyancy aids present in modern fishes[26], the mechanisms used for these earliest nektonic vertebrates for hydrodynamic lift and swimming stability remains unclear.

Recent computational simulations indicate that, during forward motion, the headshield of some ostracoderms (especially heterostracans) would act as a hydrofoil producing, unexpected, high lift forces, providing good hydrodynamic performance for efficient cruising[33,34]. These studies however do not discuss on the hydrodynamic causes of the high lift forces observed. They are based on simplified Computational Fluid Dynamics (CFD) schemes, where the governing equations are time-averaged and they do not fully resolve the nature of the flow structures in the wake of the fish. Moreover, they cover very limited dimensionless parameter spaces. Thus, a detailed flow structure and hydrodynamic forcing analysis is still missing, and in consequence, the real mechanisms associated to the hydrodynamic performance of these fish, remain unknown. Therefore, exploring the forces and the flow velocity field around the headshields turns critical to understand how vertebrates first colonized the water column and went from benthonic to pelagic forms. In this sense, a previous study, using classical flow visualization techniques, into the hydrodynamics of the Heterostracan Pteraspidiform *Errivaspis waynensis*, showed that the flow over its dorsal surface could display flow traits such as the formation of LEVs[36]. As the cephalic shields of pteraspidiformes typically showed a triangular-shaped planform, it seems intuitive that the generation of LEV dominated flow, as described in *Errivaspis waynensis* could have been a common feature among them. We hypothesize that these LEVs, if exist, could provide significant forces for hydrodynamic lift and swimming stability in earliest nektonic vertebrates.

To test this, we have investigated the hydrodynamics in real-size 3D printed models of two Early Devonian Pteraspidiformes, *Doryaspis nathorsti* and *Panamintaspis snowi* using detailed force measurements and digital particle image velocimetry (DPIV) in a water tunnel (see "Methods" section). Pteraspidiformes displayed a large variation in headshield shape. The species studied were chosen as model species for different delta-shaped planform headshield morphologies: *P. snowi* which has a streamlined body and *D. nathorsti* which present a more oblate, dorso-ventral flattened cephalic shield with large laterally expanded extensions (cornual plates). More detailed information about the studied taxa, as well as an estimation of their centre of masses, is provided in "Methods" section and in Supplementary Fig. 1. Our analyses emulate both pelagic and benthic conditions, i.e. covering the case of the fish swimming in the water column, as well as the case of swimming near a fixed boundary, in order to simulate a ground effect condition swimming (see "Methods" section and Supplementary Fig. 2).

Results

Hydrodynamic performance

Force measurements were carried out by increasing the angle of attack α, defined as the angle between the chord-line of the cephalic shield and the freestream velocity. The results of lift, drag, and moment curves as a function of angle of attack are presented in Fig. 1. The shapes of the C_L

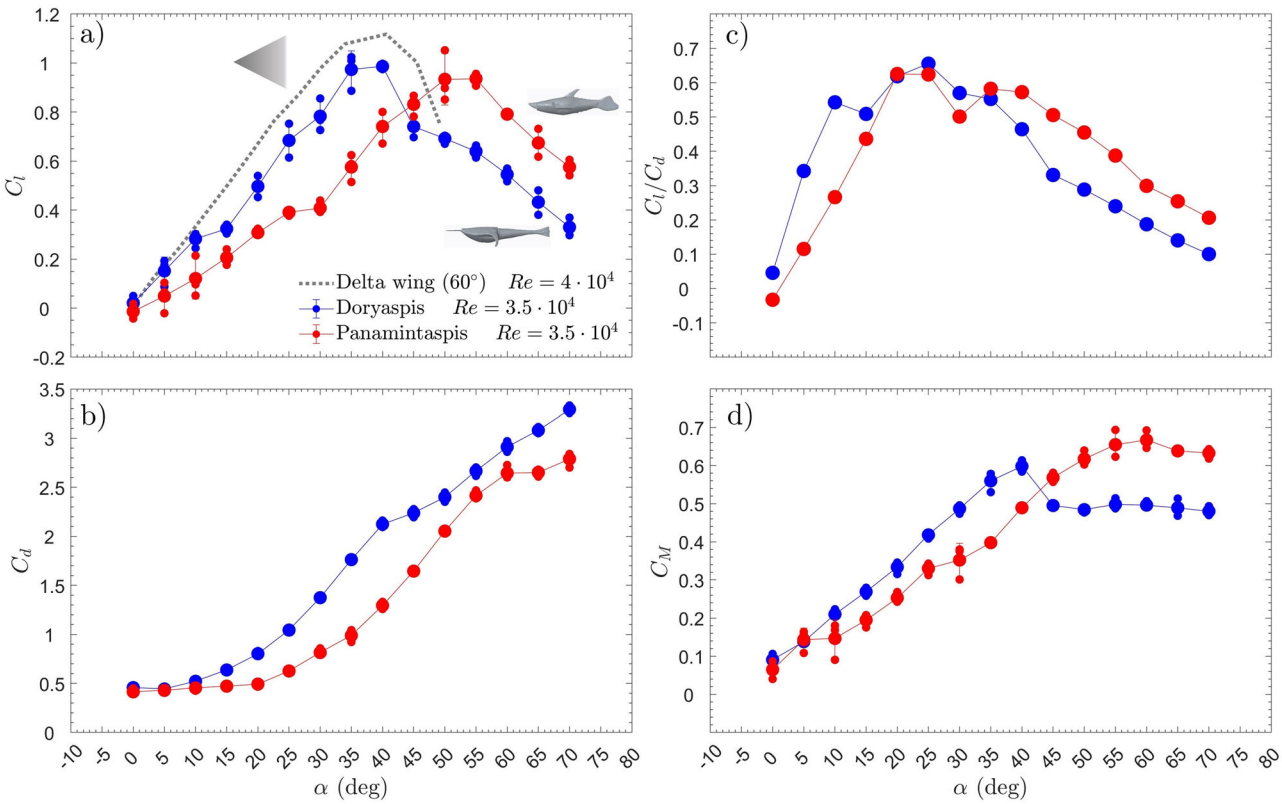

Fig. 1 | Hydrodynamic performance of Pteraspids. Coefficients of lift C_L (**a**), drag C_d (**b**), and moment C_M (**d**) together with lift to drag ratio C_L/C_d (**c**), for *D. nathorsti* is and *P. snowi* as a function of angle of attack (α), at a Re = 3.5×10^4. The dashed line in plot a), is for the lift coefficient of a delta wing with swept angle of 60° at similar Reynolds number[37] for comparison. Three experimental runs were conducted for each angle of attack. Small solid dots are for each repetition. Large solid dots are for the mean value of all repetitions and error bars indicate their standard deviation. In most of the cases, dots and error bars collapse all together around the mean value and are not visible.

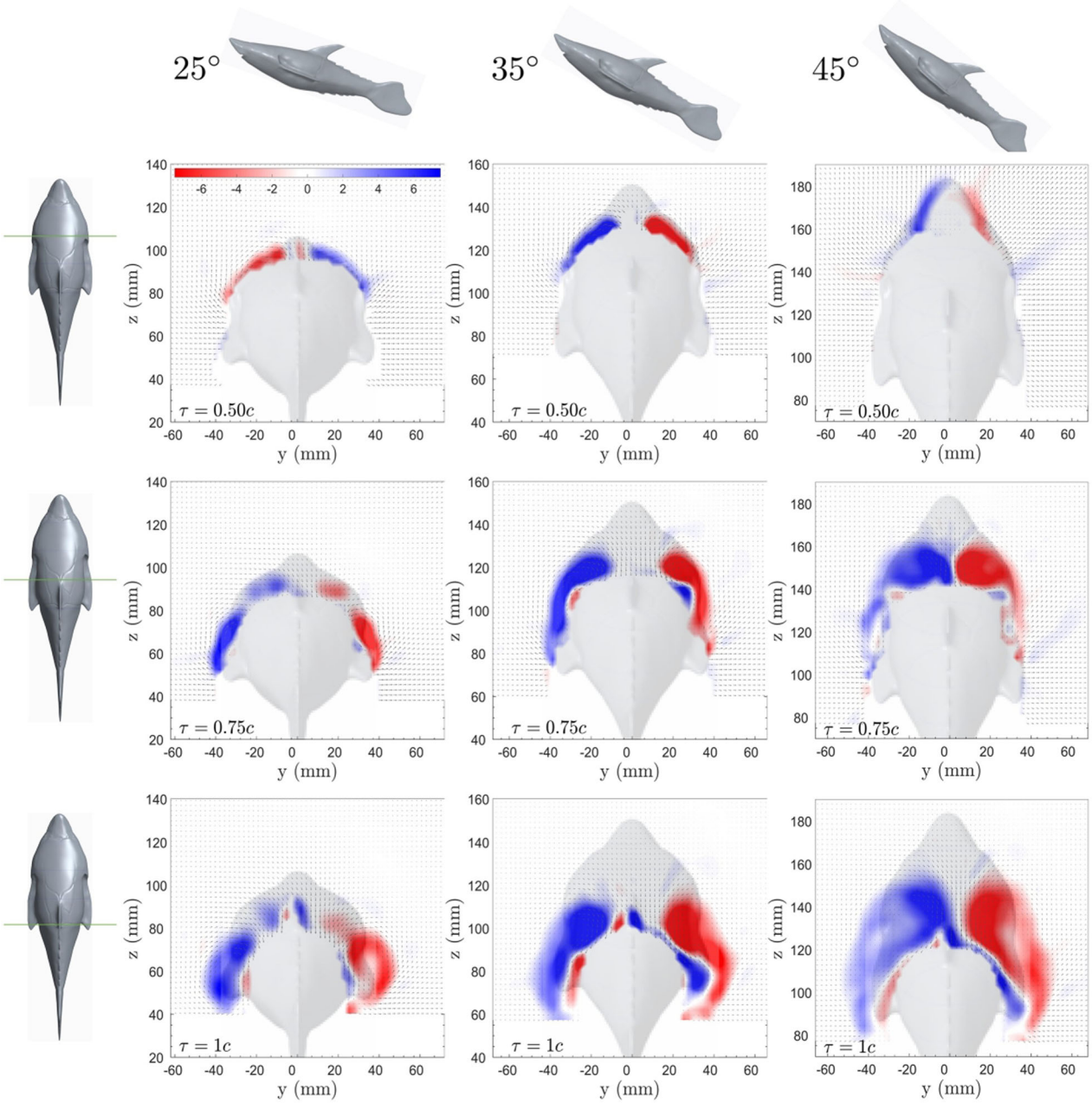

Fig. 2 | Flow structures around the headshield of *Panamintaspis snowi*. Time averaged dimensionless vorticity (ω_x c/U) fields for *P. snowi* at different angles of attack α of 25, 35, and 45 degrees (left, middle and right column, respectively), and different locations along the cephalic shield τ, at 50, 75, and 100% of the chord length (first, second, and third row, respectively), at a Re = 3.5×10^4. Blue indicates clockwise rotation and red counterclockwise.

curves for the two fishes are comparable to those of delta wings, characterized by the absence of stall at angles α, lower than 35 degrees[1]. For comparison, we show data for a delta wing with a swept angle of 60 degrees (comparable to that inferred from the fish models, see Supplementary Fig. 1) at the same regime[37], i.e. at $Re = 4 \times 10^4$. Lift force (Fig. 1a) increases monotonically up to an angle α of ~40° for *D. nathorsti*, and up to 50° for *P. snowi*, with slopes of 0.027 and 0.019 deg^{-1}, respectively. This trend is comparable to typical lift curve slope values associated with triangular delta wings, which are in the order of 0.031 deg^{-1}, as in the case of the 60° delta wing data shown. Just after reaching the highest lift value, stall takes place with the lift force decreasing abruptly. Maximum values of lift coefficient are very similar for both models, with 0.99 for *D. nathorsti* and 0.94 for *P. snowi*, and near those reached with the 60° delta wing, with a value slightly over 1.

Flow structures around the headshields

DPIV results clearly explain, from the fluid mechanics point of view, the trends observed in the lift coefficient curves. The DPIV flow visualizations (Figs. 2 and 3) show the existence of LEVs over the cephalic shield of both specimens. Both figures show time-averaged dimensionless vorticity (ω_x *c*/*U*) at different *yz* planes in different locations τ, along the chord of the cephalic shield (see Supplementary Figs. 1 and 2 for details). The flow around *P. snowi* before stall, is characterized by a pair of counter-rotating stable symmetric leading-edge vortices that develop over the head-shield of the fish. At an angle of attack of 25 deg, the vortices are elongated and flat, following the shape of the headshield until they separate from the body at the end of the cephalic shield. As the angle of attack increases, the vortices grow in size and strength, and move towards the upper part of the headshield. At larger α, not only

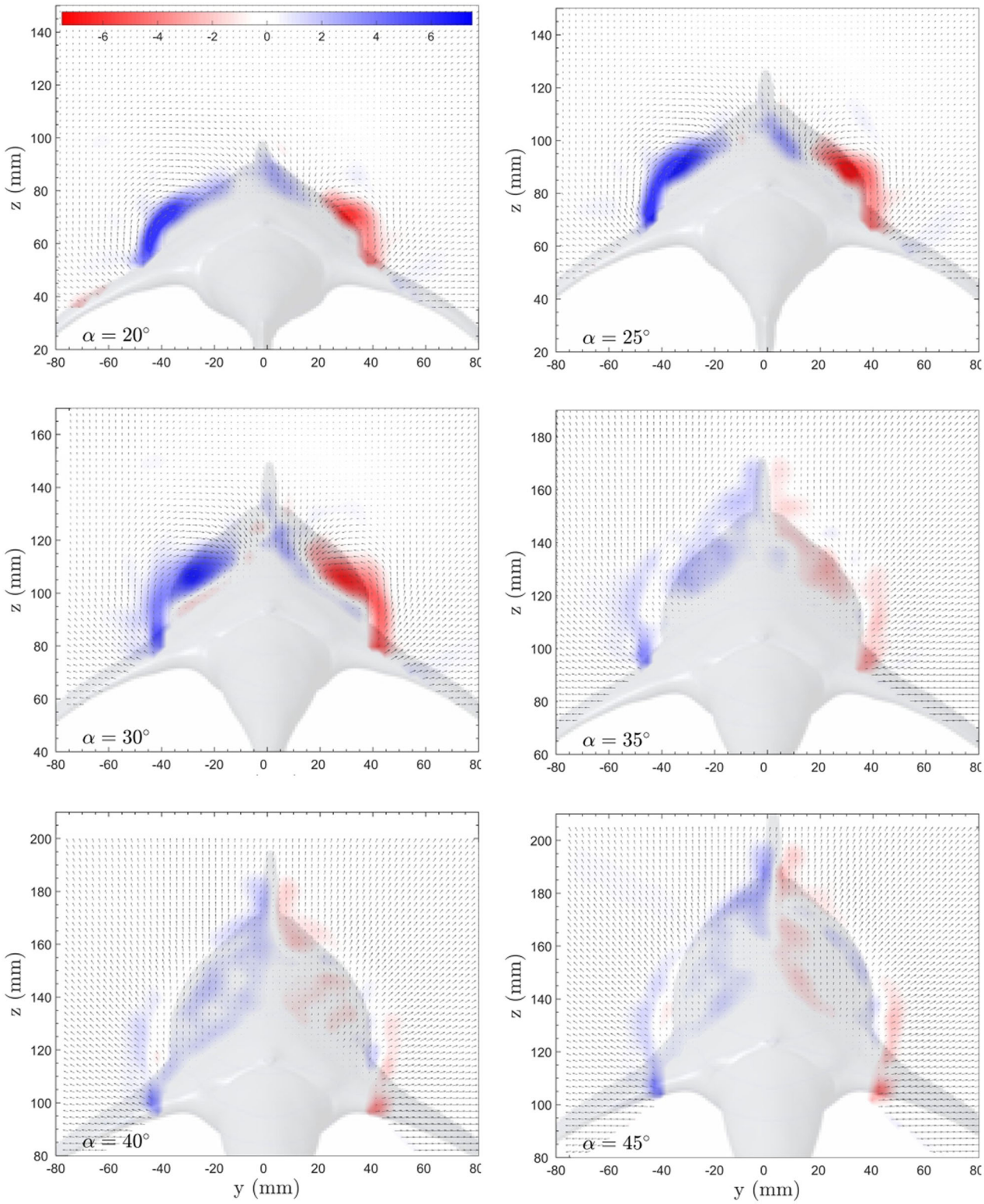

Fig. 3 | Flow structures around the headshield of *Doryaspis nathorsti*. Time averaged dimensionless vorticity (ω_x c/U) fields for *D. nathorsti* at different angles of attack α from 20 to 45 in 5 degrees steps, at a location of 0.75c on the cephalic shield, at a Re = 3.5×10^4. Blue indicates clockwise rotation and red counterclockwise.

there is increased interaction between the main vortices, but they also separate from the body earlier along the headshield. A second region of vorticity, with opposite sign with respect to the main vortex, appears between the body and the latter. Further increase of the angle of attack leads to an even earlier detachment of the body with the consequent vortex breakdown and the disorganization of the LEVs, leading to lift reduction and stall, at approximately 50 degrees (Fig. 1). In the same way, Fig. 3 shows the evolution of the flow structures around the cephalic shield of *D. nathorsti* as a function of the angle of attack. The vorticity fields show the wake at a fixed position of 75% of the chord length, as a function of the angle of attack, which was varied from 20 to 45 in steps of 5 degrees going through stall, that takes place around 35

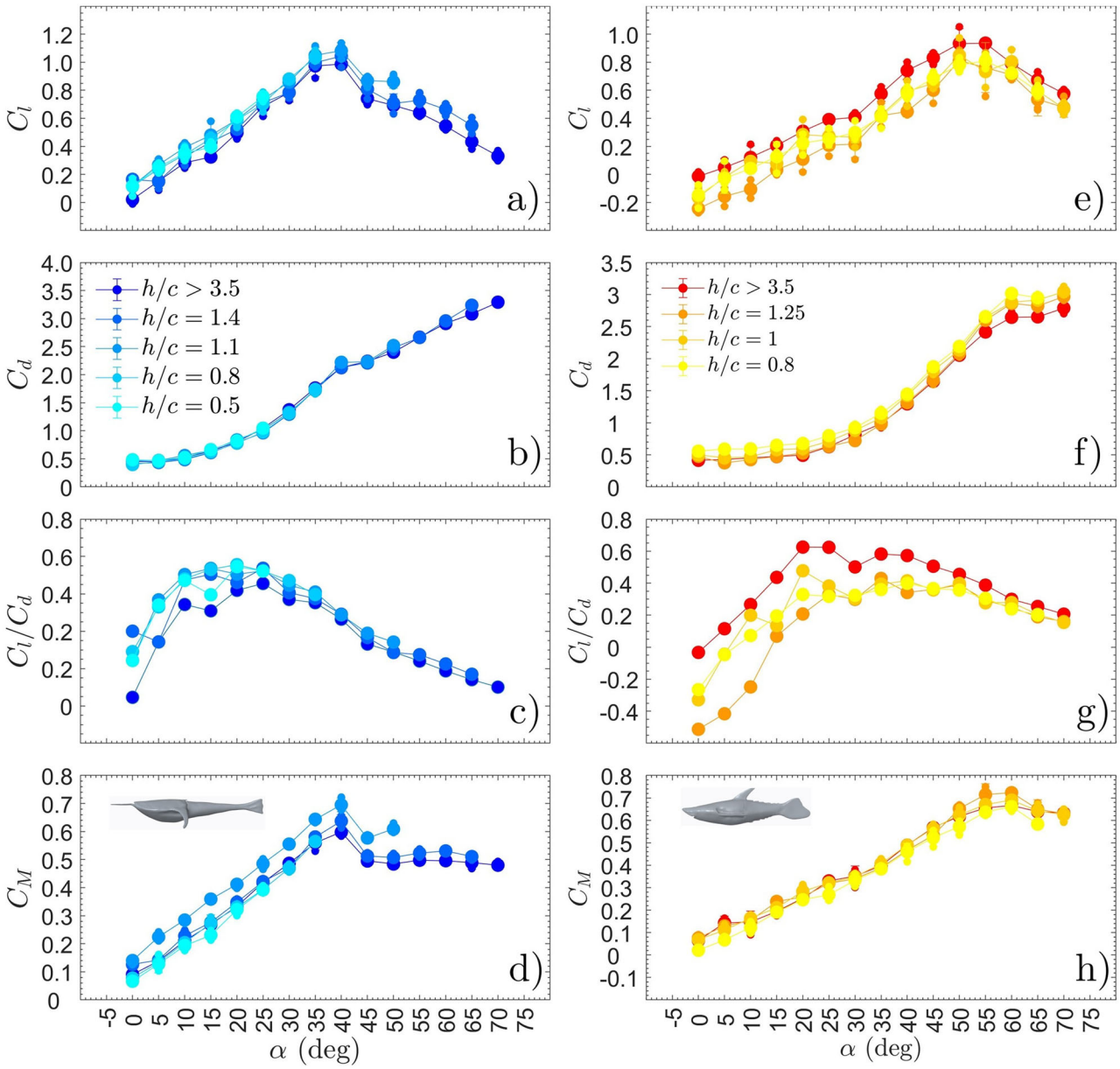

Fig. 4 | Hydrodynamics performance; benthic *vs.* pelagic scenarios. Coefficients of lift C_L (**a**, **e**), drag C_d (**b**, **f**), and moment C_M (**d**, **h**) together with lift to drag ratio C_L/C_d (**c**, **g**) for *D. nathorsti* (left column) is and *P. snowi* (right column) as a function of angle of attack (α) and the ventral distance to the ground (h/c), at a $Re = 3.5 \times 10^4$. Note that as the ventral distance is reduced, the angles of attack attainable are smaller to avoid contact of the caudal fin with the surface. Three experimental runs were conducted for each angle of attack. Small solid dots are for each repetition. Large solid dots are for the mean value of all repetitions and error bars indicate their standard deviation. In most of the cases, dots and error bars collapse all together around the mean value and are not visible.

degrees for *D. nathorsti* (Fig. 1). The vortex pair remains attached to the body up to an angle of approximately 30 degrees. At around 35 degrees of angle of attack, vortices are already disorganized and weakened. Up to this point, lift coefficient grows almost linearly and saturates at 35 where it starts its abrupt descent due to stall.

Hydrodynamic performance under benthic scenario

In order to compare the performance of the specimens in a benthic scenario, experiments were repeated by configuring different separations between the ventral region of the fish to the wall of the water channel, simulating the ground effect when near the seabed ("Methods" section, Supplementary Fig. 2). Figure 4 shows the lift, drag, moment and lift to drag curves for both specimens, as a function of the angle of attack, for the different ventral distances to the wall (h), that was varied from 0.5c to more than 3.5c (centre of the channel). Both fishes are characterized by drag coefficients that are practically unaltered independently of h. However, lift and moment coefficients undergo changes when the models approach the wall. In the case of *D. nathorsti*, (left column), lift is slightly higher when the specimen is near to the wall, yielding enhanced lift to drag ratios, especially at pre-stall angles. Conversely, *P. snowi* shows the opposite trend in lift, with lift to drag ratio reducing as the distance to the wall is decreased. These results suggest that, although both fish could perform efficiently in benthic and pelagic scenarios over a wide range of angles of attack, *D. nathorsti* showed a better hydrodynamic performance near the ground, whilst *P. snowi* did so in the water column.

Discussion

Our analysis reveals that, during forward swimming, the cephalic shield of Pteraspidiformes performed similar to delta wings, with the formation of stable LEVs over their dorsal surfaces, resulting in vortex lift forces, which

indicates that the fishes may have exhibited better hydrodynamic performance and stability than traditionally considered[21–25].

In terms of in-line force coefficients, lowest drag is achieved around zero angle of attack, with both fishes exhibiting C_D values (Fig. 1b) that remain under 0.5 for α lower than 10° (*D. nathorsti)* or 20° (*P. snowi)*. These values are comparable to those measured in actual living fish with rigid bodies, such as Ostraciidae, in which the flow is known to be dominated by LEVs[13,14], and therefore associated to a drag penalty. It is therefore expected that, during rutine swimming, they used near zero angle of attack in order to optimize the energetic cost of locomotion[38]. As the angle of attack builds up, there is a quadratic increase of drag until stall, point at which drag continues increasing but less abruptly. The lift to drag ratio (Fig. 1c) reaches maximum values near 0.65 in both fishes at an angle of attack of ~25 deg. The moment coefficient (Fig. 1d) increases monotonically in both fishes up to their respective stall angles, remaining afterwards in a plateau. In the case of *D. nathorsti* the drop in the moment coefficient associated to stall is more pronounced than in the case of *P. snowi*. Results clearly indicate that both fish were able to produce relatively large changes in lift and moment coefficients, with small changes in angle of attack whilst maintaining a moderate drag. The lift to drag ratio curve depicts high efficiency over a wide range of pre-stall angles of attack.

The high sensitivity of lift force with respect to the angle of attack evidence that rapid swimming accelerations would result in large vortex-lift forces over the fish headshield. As the upward suction effect of the LEVs, is anterior to the centre of mass, which is located at the posterior part of the headshield in both fishes (see Supplementary Information), it would promote a nose-up pitching moment[14] and, consequently, a rise in the water column.

In addition, the delta wing function of their headshield, suggests that the fishes were able to maintain extended stages of passive gliding, as evidenced by the high efficiency showed in the measured lift to drag ratio curves of both fishes. In this sense, a burst and coast swimming (i.e. a cycle with the succession of a period of active bursts followed by a passive gliding phase) has been suggested as the primitive swimming routine for earliest bentonektonik vertebrates[23,39]. This behavior is frequently observed in subcarangiform and carangiform living fishes, minimizing the global cost of transport up to 50% when compared with steady swimming[40]. Thus, a burst and coast strategy could be advantageous in terms of energy saving, in earliest foraging vertebrates which lacking jaws would have had limited energy intake, being probably detritivores and planktivores[31,39,41].

Having no fins other than the caudal one (its only movable appendage) should have played an essential role in its locomotion. Heterostracans possessed large, massive hypocercal tails[42,43] (i.e. the vertebrae/notochord bends down and extends into the ventral lobe, supporting posterodorsally the rest of the tail), which must have powered not only for thrust production but also for the generation of vertical forces and moments that allow swimming stability and control of their spatial orientation[39,43–45]. In addition, constraints of the caudal part of the body to lateral movements present in current fishes seem to be absent in ostracoderms, where many degrees-of-freedom for horizontal (dorso-ventral) flexion[45] would be present for active trimming. Thus, the high lift and moment sensitivity to angle of attack measured in our experiments, combined with initial moments produced from the caudal fin for pitch, roll or yaw, could have been exploited by Heterostracans to efficiently move in the water column. Certainly, the evolutionary emergence of paired fins in gnatostomates largely expanded the capabilities for generating hydrodynamic stabilizing forces[35,45–49], and ultimately replaced the role of the tail for this purpose[45]. However, the ability to control thrust using the tail, both for maneuvers and stability, remains important in many groups of aquatic vertebrates, including current agnathans fishes[45,50].

In summary, leading-edge vortices have been revealed to be a central unstable aero-hydro-dynamic mechanism to understand flying and swimming locomotion in several groups of current organisms[4–15]. We show here that exploiting the lift forces resulting from LEVs could have also played a critical role for earliest vertebrates, in order to first colonize the pelagic realm, more than 400 million years ago. Thus, from more ancestral vertebrate benthic forms, with robust rounded-ovalated headshield, new morphologies with delta-shaped planform headshields, evolved separately during Silurian, in most of the armoured jawless stem-gnathostomes lineages, particularly within the Heterostracans[18,19]. Our results reveal that because of their delta wing function, these headshields attain high lift forces by creating a pair of stable symmetric leading-edge vortices as they move forward, allowing the fishes to perform rapid take-offs from the sea bottom, when sudden bursts of swimming become coupled with pitch moments generated from the hypocercal caudal fin. Probably, first stages of vertebrate occupation of the water column occurred in shallow marine environments and were limited to punctual rising of essentially benthonic fishes, when escaping from predators of the saturated benthic zone, toward the still predator-free pelagic zone. This ascent in the water column would be followed by a phase of, rather erratic gliding until re-settling in a new area of the benthic zone. The hydrodynamic performance found in *D. nathorsti* fit well with this strategy and agrees with previous morphofunctional interpretations which indicated that the anatomy of *Doriaspis* (e.g. flat dorsal shield, ventral pseudorostrum, long cornual plates) could be compatible with both a pelagic and a benthic mode of life[51]. More evolved Heterostracans, with highly streamlined headshields, such as *Panamintaspis*, could already be adapted to a fully pelagic life, exploiting the LEVs forces to swim in a burst and coast mode. Consequently, differences in the hydrodynamic performance induced by the shape of their rigid headshields would be related with the first mayor ecological diversification among early vertebrates, including the emergence of first nektonic forms.

Methods

Fish models

The fish models are real-size reconstructions of the Pteraspidiformes *Doryaspis nathorsti* and *Panamintaspis snowi* (Supplementary Fig. 1). Pteraspidiformes (Heterostraci) are clade of extinct (Silurian to Devonian) armoured jawless fishes which are among the oldest vertebrates known[18,52,53]. They are characterized by having a large, rigid external shield enclosing the head and anterior part of the body, composed of several independent cephalic plates separated by sutures, including paired cornual plates and an independent dorsal spine (see "Methods" section, Supplementary Fig. 1). The rest of the body and the caudal fin are covered by small scales. A single, common external branchial opening, characterized by a branchial plate, is present on either side of the head armour, near the cornual plates. The mouth is surrounded by elongated, and probably moving plates. Most Pteraspidiformes show streamlined bodies, having a fusiform cephalic shield, which is ventrally bulged, dorsally more flattened and have a triangle-shaped planform with an elongated rostral plate, and a distally flexible body. They also present a system of deep, closed canals on the dorsal disc, probably related to sensorial organs[18]. An accurate revision on the phylogeny of the Pteraspidiformes[52,53] as well as more detailed morphological descriptions of *Panamintaspis snowi*[54] and *Doryaspis nathorsti*[55] can be found in the literature. *P. snowi* is know from marine strata of the Lost Burro Formation (California, USA), interpreted as an estuarine environment. *D. nathorsti* occurs in semi-continental deposits (fjords or estuaries) with significant fluvial continental contributions from the Wood Bay Formation (Norwegian Svalbard archipelago, Spitsbergen)

Physical models of both fish were 3D printed in PolyLactic Acid (PLA) based on Computer Aided Design (CAD) models, obtained from morphological reconstructions and on the study of fossil specimens held at the Muséum National d'Histoire Naturelle, Paris. CAD models were also used to obtain reference areas (*S*) for each fish, needed to compute the dimensionless force and moment coefficients. The planform area of the rigid cephalic shield resulted in 66.05 cm^2 for *Doryaspis nathorsti* and 75.63 cm^2 for *Panamintaspis snowi*. Frontal areas are 29.17 and 26.59 cm^2, respectively. Chord lengths were precisely obtained from the CAD models, resulting in 101 mm for *Doryaspis nathorsti* and 134 mm for *Panamintaspis snowi*. The approximate sweep angle estimated for *D. nathorsti* is 50° and for *P. snowi* 60° (Supplementary Fig. 1).

Centre of mass and buoyancy estimations

The centres of mass and buoyancy of the studied fishes were approximated using the available reconstructions of the Heterostraci[18,56] which are mostly based on fossilized internal casts of the head armour (i.e. impressions of the brain, pineal organ, semicircular canals, gill chambers, and muscle attachments). The position of the centres of mass and buoyancy, as well as the body volume, were calculated by taking regularly spaced slices in a computer generated 3-D reconstruction[57] and assigning the appropriate densities to the different tissues, i.e., 2000 kg m^{-3} for the skeleton, 1060 kg m^{-3} for the muscles, 1000 kg m−3 for the other soft parts and 1020 kg m^{-3} (about the density of sea water) for the mouth cavity and the branchial tubes.

With these values, approximately 80% of the volume and 81% of the mass of the *D. nathorsti* corresponded to the armoured head. The centre of mass has been estimated at 76% of the chord (0.76c) measured from the start of the tip of the animal, with its center of buoyancy very close. In the case of *P. snowi*, the volume of the cephalic shield accounted for 76% of the total volume and a 76% of the total mass of the fish, with its centre of mass located at 72% of the chord (0.72c) from the tip (Supplementary Fig. 1).

Experimental setup

Experiments were conducted in the free surface water channel (FSWC) of the Laboratory for Fluid–Structure Interactions (LIFE) at Universitat Rovira i Virgili (URV) in Tarragona. The water channel has a cross-section of 1×1.1 m^2 downstream of a 6 to 1 three-dimensional contraction (cross-sectional area), and can deliver a flow rate over 0.5 m^3/s. The length of the working section is 2.25 m and it is made of glass, especially designed for the use optical measurement techniques. The flow is generated by two axial pumps controlled by two frequency sources. The flow profile in the working section is characterized by very low variability in the velocity, with a maximum deviation in cross-sectional planes of 1.58%. The blockage, i.e. the ratio of the frontal area of the models to the cross-section of the water channel for these experiments was very low (< 0.5%) and the set-up was designed to have the fish model at the middle of the water channel minimizing free surface and wall effects. The experimental design permitted the positioning of the models at different horizontal distances (h) to the side wall of the channel to study ground effect in the desired cases, as explained in the main document. The distance h is measured from the ventral attachment of the fish to the side wall of the channel, and experiments were conducted for different separation distances in the range from 0.2 to more than 3.5 chords (centre of the channel condition).

A Cartesian reference frame is defined with the x axis aligned to the flow and in the same direction, the z perpendicular to the flow and to the bottom of the water channel and finally the y, axis perpendicular to both. The models were placed in the channel rotated 90 degrees around the x axis and attached to a 6 mm stainless steel rod on their bottom, allowing the upper part of the fish, where the leading-edge vortices appear, to be free of any element causing flow interference. The rod runs inside a 20×20 mm aluminum beam that provides rigidity and high natural frequencies to the system. The beam is enclosed inside a 3D printed NACA 0015 profile that streamlines the support and minimizes its wake, eliminating any flow-induced vibrations of the system. At the upper end of the rod, outside the water tank, there is a specially designed 3D printed part that allows to mechanically configure the angle of attack (α) of the model in steps of 5 degrees, by rotating the rod to which the fish is attached. This way, although the fish rotates to the desired position, the NACA profile always remains parallel to the flow. The set-up allows to configure the angle of attack precisely and repetitively before starting each measurement. The support system hangs from a 6 degree of freedom (DOF) balance which is attached to a planar (xy) air bearing rig. One of the frictionless directions of the air bearing rig is parallel to the flow direction (x) and the other is perpendicular (y). If not restricted to move, the model could translate without friction in any of the two directions because of the action of the hydrodynamic forces acting on the body. Nevertheless, motion is restricted using two uni-axial load cells aligned to each direction directly providing measurements of drag and lift on the fish model. Therefore, force measurements were obtained redundantly with two completely independent measurement systems: the 6 DOF balance and the precision uni-axial load cells aligned to the air bearing directions. This mechanical design has been used in several previous recent experiments carried out in the facility[58–61] and was installed here, for validation purposes only. Comparisons between drag and lift obtained using these two independent measurement methods showed excellent agreement. Schematic views of the experimental setup appear in Supplementary Fig. 2.

Data acquisition

All signals were sampled at 2 kHz for a period of at least 90 s. For each fish model, tests were carried out varying the angle of attack from 0 to more than 60 in steps of 5 degrees. The experiments were conducted by generating realistic Reynolds numbers (Re) based on the cephalic chord, of 3.5×10^4 for both models, after setting a flow speed in the water channel of 0.4 m/s in the case of *P. snowi* and 0.3 m/s for *D. nathorsti*. Reynolds number gives the ratio of inertial forces to viscous forces (Uc/v), with U being the free-stream velocity in the water channel, c the cephalic chord length, v the kinematic viscosity of water. Hydrodynamic forces acting on the models are expressed using dimensionless coefficients of drag (C_D), lift (C_L) and moment (C_M). Force coefficients were computed by dividing the time-averaged force (drag or lift) by the dynamic pressure, multiplied by a reference area ($0.5\rho U^2 S$). The reference area (S) is the planform cephalic area when calculating lift, and the frontal area in the case of drag coefficient. Moment is expressed in dimensionless form using the planform area multiplied by the chord.

Initially, the experiments were conducted with the models placed at the centre of the water channel, away from the influence of the walls, with a separation to those of more than 3.5 chords. We have also studied the hydrodynamic performance of the fish in benthic scenarios, by repeating the experiments with the models near the wall of the water channel, at different distances (h), to explore the effects of the boundary on the hydrodynamic forces. Results showing the force coefficients obtained during the experiments are shown in Figs. 1 and 4 of the main document.

Digital particle image velocimetry

In order to study the flow around the fish models, time-resolved DPIV[62,63] was used in some specific cases of interest. Images were recorded at 500 Hz using a CCD-sensor with 12-bit resolution, a pixel size of 10 mm and 1280×1024 pixels, in combination with a lens with 35 mm fixed focal length. The flow in the water channel was seeded using 20 micron neutrally buoyant polyamide particles and the illumination was generated using a continuous wave (CW) diode-pumped solid state (DPSS) green laser, able to deliver up to 5 W. A mirror was installed inside the water channel at an angle of 45 degrees with respect to the flow direction, downstream the model and well apart from it, to avoid any flow interference. This was used to capture images of the laser illuminated flow particles at different yz cross-sectional planes (τ) along the cephalic shield of the models. The planes, that appear indicated in Supplementary Fig. 1, were perpendicular to the flow direction at several distances, namely 25, 50, 75, and 100% of the chord, along the length of the cephalic shields of the fish models. Image pre-processing using MATLAB scripts was performed to mask regions without particles in the flow and to identify in each DPIV snapshot the position of the model. After this initial processing, a fast Fourier transform (FFT) cross-correlation algorithm[57] was applied to the pre-processed images, using an interrogation area 32×32 pixels with a 50% area overlap. Spurious vectors produced by the cross-correlation scheme were threshold and replaced by new values obtained from neighboring interpolation. Post-processed results prepared using MATLAB scripts, showing velocity vectors together with vorticity colormaps overlapping the 3D model of the fish, are shown in Figs. 2 and 3.

Statistics and reproducibility

MATLAB scripts have been used to process and visualize all the experimental data. The data processing includes the application of the offsets, sensitivities, and calibration matrices of the sensors used for the measurements, as well as the computation of all the parameters included in the figures, such as the time-averaged values of hydrodynamic coefficients

presented in Fig. 1 and Fig. 4. MATLAB scripts have been also used for generating all the plots presented in the manuscript. All water tunnel runs were repeated a minimum of three times, and error bars in the plot indicate the standard deviation of the mean values obtained in each experiment. In general, all reported values in the plots derived from the experiments have standard deviations similar to the marker size.

Reporting summary

Further information on research design is available in the Nature Portfolio Reporting Summary linked to this article.

Data availability

All tabulated data used to make figures are available in perpetuity at: https://osf.io/ycs7m/?view_only=08ef8c0118424dc98f1483e179ec1e21.

Received: 27 October 2023; Accepted: 4 September 2024;
Published online: 16 September 2024

References

1. Anderson, J. D. *Fundamentals of Aerodynamics*. ed. 4 (McGraw-Hill, 2005).
2. Gursul, I., Gordnier, R. & Visbal, M. Unsteady aerodynamics of non-slender delta wings. *Prog. Aerosp. Sci.* **41**, 515–557 (2005).
3. Ol, M. V. & Gharib, M. Leading-edge vortex structure of nonslender delta wings at low Reynolds Number. *AIAA J.* **41**, 16–26 (2003).
4. Maxworthy, T. The fluid dynamics of insect flight. *Ann. Rev. Fluid Mech.* **13**, 329 (1981).
5. Ellington, C. P. et al. Leading-edge vortices in insect flight. *Nature* **384**, 626 (1996).
6. Dickinson, M. H., Lehmann, F.-O. & Sane, S. P. Wing rotation and the aerodynamic basis of insect flight. *Science* **284**, 1954 (1999).
7. Srygley, R. B. Unconventional lift-generating mechanisms in free-flying butterflies. *Nature* **420**, 660 (2002).
8. Muijres, F. T. et al. Leading-edge vortex improves lift in slow-flying bats. *Science* **319**, 1250 (2008).
9. Johansson, L. C. et al. Ear-body lift and a novel thrust generating mechanism revealed by the complex wake of brown long-eared bats (*Plecotus auritus*). *Sci. Rep.* **6**, 24886 (2016).
10. Videler, J. J., Stamhuis, E. J. & Povel, G. D. E. Leading-edge vortex lifts swifts. *Science* **306**, 5703 (2004).
11. Warrick, D. R., Tobalske, B. W. & Powers, D. R. Aerodynamics of the hovering hummingbird. *Nature* **435**, 1094–1097 (2005).
12. Lentink, D. et al. Leading-edge vortices elevate lift of autorotating plant seeds. *Science* **324**, 1438 (2009).
13. Bartol, I. K. et al. Body-induced vortical flows: a common mechanism for self-corrective trimming control in boxfishes. *J. Exp. Biol.* **208**, 327 (2005).
14. Marcroft, T. et al. Boxfish swimming paradox resolved: forces by the flow of water around the body promote manoeuvrability. *J. R. Soc. Interface* **46**, 1146 (2014).
15. Johansson, L. C. & Norberg, R. Å. Delta-wing function of webbed feet gives hydrodynamic lift for swimming propulsion in birds. *Nature* **424**, 65 (2003).
16. Mayburylt, W. J., Rayner, J. M. V. & Couldrick, L. B. Lift generation by the avian tail. *Proc. R. Soc. Lond. B* **268**, 1443–1448 (2001).
17. Dyke, J., Nudds, R. L. & Rayner, J. M. V. Flight of *Sharovipteryx mirabilis*: the world's first delta-winged glider. *J. Evol. Biol.* **19**, 1040–1043 (2006).
18. Janvier, P. *Early Vertebrates* (Oxford Univ. Press, 1996).
19. Blieck, A. Biodiversité, environnements et évolution au Paléozoïque : le cas des vertébrés du Cambrien au Dévonien (- 542 à - 359 Ma) [Palaeozoic biodiversity, environments and evolution: the case of Cambrian to Devonian vertebrates (-542 to -359 My)]. *Ann. Soc. Géol. Nord, 2e série* **16**, 19–33 (2009). [In French with English abstract].
20. Donoghue, P. C. J. & Keating, J. N. Early vertebrate evolution. *Front. Palaeontol.* **57**, 5 (2014).
21. White, E. I. The ostracoderm *Pteraspis* Kner and the relationships of the agnathous vertebrates. *Philos. Trans. R. Soc. B* **225**, 381–457 (1935).
22. Nursall, J. R. Swimming and the origin of paired appendages. *Am. Zool.* **2**, 127–141 (1962).
23. Aleyev, Y. G. *Nekton* (The Hague, 1977).
24. Aleyev, Y. G. & Novitskaya. L. I. An experimental study of the Hydrodynamic characteristics of Devonian Heterostraci. *Paleontol. J.* **1**, 3 (1983) [in Russian].
25. Pernègre, V. N. & Elliott, D. K. Phylogeny of the pteraspidiformes (heterostraci), silurian-devonian jawless vertebrates. *Zool. Scr.* **37**, 391–403 (2008).
26. Alexander, R. M. Size, speed and buoyancy adaptations in aquatic animals. *Am. Zool.* **30**, 189–196 (1990).
27. Klug, C. et al. The Devonian nekton revolution. *Lethaia* **43**, 465–477 (2010).
28. Anderson, P. S. L. et al. Initial radiation of jaws demonstrated stability despite faunal and environmental change. *Nature* **476**, 206–209 (2011).
29. Whalen, C. D. & Briggs, D. E. G. The Palaeozoic colonization of the water column and the rise of global nekton. *Proc. R. Soc. B* **285**, 20180883 (2018).
30. Blieck, A. From adaptive radiations to biotic crises in Palaeozoic vertebrates: a geobiological approach. The André Dumont medallist lecture. *Geol. Belg.* **14**, 203–227 (2011).
31. Purnell, M. A. Feeding in extinct jawless heterostracan fishes and testing scenarios of the early vertebrate evolution. *Proc. R. Soc. B* **269**, 83–88 (2002).
32. Sallan, L. et al. The nearshore cradle of early vertebrate diversification. *Science* **362**, 460–464 (2018).
33. Ferrón, H. G. et al. Computational fluid dynamics suggests ecological diversification among stem-gnathostomes. *Curr. Biol.* **30**, 4808–4813 (2020).
34. Dec, M. Hydrodynamic performance of psammosteids: New insights from 465 computational fluid dynamics simulations. *Acta Palaeontol. Pol.* **64**, 679–684 (2019).
35. Fish, F. E. & Lauder, G. V. Control surfaces of aquatic vertebrates: active and passive design and function. *J. Exp. Biol.* **220**, 4351–4363 (2017).
36. Botella, H. & Fariña, R. A. Flow pattern around the rigid cephalic shield of the Devonian agnathan *Errivaspis waynensis* (Pteraspidiformes: Heterostraci). *Palaeontology* **51**, 1141–1150 (2008).
37. Traub, L. W., Moeller, B. & Rediniotis, O. Low-Reynolds-Number effects on delta-wing aerodynamics. *J. Aircr.* **35**, 653–656 (1998).
38. He, P. & Wardle, C. S. Tilting behavior of the Atlantic mackerel, Scomber scombrus, at low swimming speeds. *J. Fish. Biol.* **29**, 223–232 (1986).
39. Webb, P. W. & Smith, G. R. Function of the caudal fin in early fishes. *Copeia* **1980**, 559–562 (1980).
40. Fish, F. E. *Fish locomotion: An eco-ethological perspective* (ed. Domenici, P) 90-122 (CRC Press, 2010).
41. Mallatt, J. Feeding ecology of the earliest vertebrates. *Zool. J. Linn. Soc.* **82**, 261–272 (1984).
42. Pradel, A. et al. The tail of the Ordovician fish. *Sacabambaspis. Biol. Lett.* **3**, 72–75 (2007).
43. Mark-Kurik, E. & Botella, H. On the tail of *Errivaspis* and the condition of the caudal fin in heterostracans. *Acta Zool.* **90**, 44–51 (2009).
44. Kermack, K. A. The functional significance of the hypocercal tail in *Pteraspis rostrata*. *J. Exp. Biol.* **20**, 23–27 (1943).
45. Webb, P. W. Control of posture, depth, and swimming trajectories of fishes. *Int. Comp. Biol.* **42**, 94–101 (2002).
46. Harris, J. E. The role of fins in the equilibrium of swimming fish. I. Wind-tunnel tests on a model of *Mustelus canis* (Mitchill). *J. Exp. Biol.* **13**, 474–493 (1936).

47. Fish, F. E. & Shannahan, L. D. The role of the pectoral fins in body trim of sharks. *J. Fish Biol.* **56**, 1062–1073 (2000).
48. Wilga, C. D. & Lauder, G. V. Three-dimensional kinematics and wake structure of the pectoral fins during locomotion in leopard sharks *Triakis semifasciata*. *J. Exp. Biol.* **203**, 2261–2278 (2000).
49. Webb, P. W. & Weihs, D. Stability versus maneuvering: challenges for stability during swimming by fishes. *Int. Comp. Biol.* **55**, 753–764 (2015).
50. Ullén, F. T. et al. Spatial orientation in the lamprey. I. Control of pitch and roll. *J. Exp. Biol.* **198**, 665–673 (1995).
51. Pernègre, V. N. Description d'une nouvelle espèce et analyse morpho-fonctionnelle du genre *Doryaspis* White (Heterostraci) du Dévonien du Spitsberg. *Geobios* **38**, 257–268 (2005).
52. Randle, E. & Sansom, R. S. Exploring phylogenetic relationships of Pteraspidiformes heterostracans (stem- gnathostomes) using continuous and discrete characters. *J. Syst. Palaeontol.* https://doi.org/10.1080/14772019.2016.1208293 (2016).
53. Randle, E. & Sansom, R. S. Phylogenetic relationships of the 'higher heterostracans' (Heterostraci: Pteraspidiformes and Cyathaspididae), extinct jawless vertebrates. *Zool. J. Linn. Soc.* https://doi.org/10.1093/zoolinnean/zlx025 (2017).
54. Elliott, D. K. & Ilyes, R. R. New Early Devonian pteraspidids (Agnatha, Heterostraci) from Death Valley National Monument, southeastern California. *J. Paleontol.* **70**, 152 (1996).
55. Pernègre, V. N. The genus Doryaspis White (Heterostraci) from the Lower Devonian of Vestspitsbergen. *Svalbard J. Vert. Paleontol.* **22**, 735–746 (2002).
56. Janvier, P. *Patterns of Structural and Systematic Diversity* (The Skull) (eds. J. Haken, J. & Hall, B. K.) pp. 131-188 (University of Chicago Press, 1993)
57. Henderson, D. M. Estimating the masses and centers of mass of extinct animals by 3-D mathematical slicing. *Paleobiology* **25**, 88–106 (1999).
58. Huera-Huarte, F. J. Dynamics and excitation in a low mass-damping cylinder in cross-flow with side-by-side interference. *J. Fluid Mech.* **850**, 370–400 (2018).
59. Huera-Huarte, F. J. Vortex-induced vibrations of a low mass-damping rigid circular cylinder with forced periodic rotations. *Phys. Rev. Fluids* **5**, 124701 (2020).
60. Huera-Huarte, F. J. & Gharib, M. Role of the near tip region of a fin on fish propulsion. *Phys. Rev. Fluids* **4**, 063103 (2019).
61. Huera-Huarte, F. J. Propulsive performance of a pair of pitching foils in staggered configurations. *J. Fluids Struct.* **81**, 1–13 (2018).
62. Willert, C. E. E. & Gharib, M. Digital Particle Image Velocimetry. *Exp. Fluids* **10**, 181–193 (1991).
63. Raffel, M.et al. *Particle Image Velocimetry: A Practical Guide* (Springer, 2018).

Acknowledgements

We thank Z. Wang and I. Gursul (University of Bath) for constructive help in the conception, and discussion of the initial experiments. A. Pradel (MNHN, Paris) for providing specimen access. Posthumous gratitude to Prof. Alain Blieck who kindly helped with the accurate morphology of pteraspids models. This work was supported by grants 2017 SGR 1263 (AGAUR), PID2021-128441NB-I00, PID2020-118642GB-I00, and PRX22/00090 (*Agencia Estatal Investigación*, Spanish government).

Author contributions

This study was conceived by H.B. and R.F.; F.H.H. designed and constructed the apparatus, performed the experiments, and collected the data; F.H.H. processed the data and produced the results and graphs; H.B and F.H.H. drafted the manuscript; all authors contributed to data interpretation and manuscript preparation.

Competing interests

The authors declare no competing interests.

Additional information

Supplementary information The online version contains supplementary material available at https://doi.org/10.1038/s42003-024-06837-8.

Correspondence and requests for materials should be addressed to Francisco Huera-Huarte.

Peer review information *Communications Biology* thanks Alan Pradel and the other, anonymous, reviewer(s) for their contribution to the peer review of this work. Primary Handling Editors: Borja Figueirido and Johannes Stortz.